Astronomy & Astrophysics manuscript no. Sr˙nlte˙astroph
December 19, 2012

Strontium: To LTE or non-LTE that is the question

The NLTE chemical evolution of Sr in extremely metal-poor stars

C. J. Hansen[1], M. Bergemann[2], G. Cescutti[3], P. Francois[4], A. Arcones[5], A. I. Karakas[6], K. Lind[2], and C. Chiappini[3]

[1] Landessternwarte, ZAH, Königstuhl 12, 69117 Heidelberg, Germany

[2] Max-Planck Institute for Astrophysics, Karl-Schwarzschild Str. 1, 85741, Garching, Germany

[3] Leibniz-Institut für Astrophysik Potsdam (AIP), An der Sternwarte 16, D-14482 Potsdam, Germany

[4] GEPI, Observatoire de Paris, CNRS Universite Paris Diderot, Place Jules Janssen, 92190 Meudon, France

[5] TU Darmstadt, Institut für Kernphysik Theoriezentrum, Schlossgartenstr. 2, 64289 Darmstadt, Germany

[6] Research School of Astronomy & Astrophysics, Mount Stromlo Observatory, Weston Creek ACT 2611, Australia

Received 18/10/2012 / Accepted 11/12/2012

ABSTRACT

Context. Strontium has proven itself to be one of the most important neutron-capture elements in the study of metal-poor stars. Thanks to the strong absorption lines of Sr, they can be detected even in the most metal-poor stars and also in low-resolution spectra. However, we still cannot explain the large star-to-star abundance scatter we derive for metal-poor stars.
Aims. Here we confront Galactic chemical evolution (GCE) with improved abundances for Sr I and Sr II including updated atomic data, to evaluate possible explanations for the large star-to-star scatter at low metallicities.
Methods. We derive abundances under both local thermodynamic equilibrium (LTE) and non-LTE (NLTE) for stars spanning a large interval of metallicities as well as a broad range of other stellar parameters. Gravities and metallicities are also determined in NLTE. We employ MARCS stellar atmospheres and MOOG for the LTE spectrum synthesis, while MAFAGS and DETAIL were used to derive the NLTE abundances. We verified the consistency of the two methods in LTE.
Results. We confirm that the ionisation equilibrium between Sr I and Sr II is satisfied under NLTE but not LTE, where the difference between neutral and ionised Sr is on average ~ 0.3 dex. We show that the NLTE corrections are of increasing importance as the metallicity decreases. For the stars with [Fe/H] > -3 the Sr I NLTE correction is $\sim 0.35/0.55$ dex in dwarfs/giants, while the Sr II NLTE correction is $< \pm 0.05$ dex.
Conclusions. On the basis of the large NLTE corrections to Sr I, Sr I should not be applied as a chemical tracer under LTE, while it is a good tracer under NLTE. Sr II, on the other hand, is a good tracer under both LTE and NLTE (down to [Fe/H] ~ -3), and LTE is a safe assumption for this majority species (are NLTE corrections not available). However, the Sr abundance from Sr II lines is dependent on an accurate surface gravity determination, which can be obtained from NLTE spectroscopy of Fe lines or from parallax measurements. We could not explain the star-to-star scatter (which remains under both LTE and NLTE) by the use of the Galactic chemical evolution model, since the Sr yields to date are too uncertain to draw firm conclusions. At least two nucleosynthetic production sites seem necessary in order to account for this large scatter.

Key words. stars: abundances – nuclear reactions, nucleosynthesis, abundances – Galaxy: evolution

1. Introduction

Strontium is one of the two neutron-capture elements (namely strontium and barium - Ba) that show intrinsically very strong absorption lines even in metal-poor stars. At solar metallicity Sr is synthesised by a variety of nucleosynthetic sources including the weak slow neutron-capture (s-) process that occurs in massive stars (e.g. Heil et al. 2009; Pignatari et al. 2010) and in AGB stars (Travaglio et al. 2004). In comparison, the production of Ba is dominated by the s-process occurring in low-mass AGB stars (Käppeler et al. 1989; Busso et al. 1999; Sneden et al. 2008). This picture changes at low metallicity, where Ba may be formed by a main rapid neutron-capture process and Sr by a charged particle process (Hoffman et al. 1997). Additionally, very metal-poor rapidly rotating massive stars might be significant producers of Sr and Ba via the s-process (Pignatari et al. 2008; Chiappini et al. 2011; Frischknecht et al. 2012). This may modify the presumption of pure r-process patterns in ultra metal-poor (UMP; $-5 <$ [Fe/H] < -4 cf. Beers & Christlieb (2005)) stars. For this reason, disentangling the nucleosynthetic origin of Sr and Ba in metal-poor stars would help us to understand the formation and evolution of the early Galaxy.

Only the 4077 Å Sr II line remains detectable in both dwarfs and giants both in high- and low-resolution spectra of metal-poor stars. Studying this line thus provides a unique insight into the behaviour of neutron-capture elements at all metallicities and spectral resolutions, ranging from the low-resolution LAMOST survey to the high-resolution Gaia-ESO survey[1]. Clearly, accurate abundances are needed in order to fully comprehend the

[1] The Sr II line is detectable if a blue setting is used for Gaia-ESO follow-up observations.

chemical evolution of Sr. This means that the effects of non-local thermodynamic equilibrium (NLTE) and deviations from hydrostatic equilibrium (3D) must be taken into account in element abundance calculations, if we want to extract the correct information from the future surveys' large flow of data. Clearly, such calculations are a challenge, as was recently demonstrated for O (González Hernández et al. 2010), Ca (Spite et al. 2012), Fe (Bergemann et al. 2012a), and for Ba (Dobrovolskas et al. 2012), while Bonifacio et al. (2009) provide 3D corrections for a large number of elements for dwarfs. The estimates of 3D effects for the Sr II resonance lines have been provided by Collet et al. (2007), who performed LTE calculations with 3D radiative-hydrodynamics simulations of stellar convection for the metal-poor stars. The 3D LTE corrections are on the order of −0.15 dex, with respect to 1D LTE. The NLTE abundances of Sr were reported in a few studies, among those, Belyakova & Mashonkina (1997), Mashonkina et al. (1999), Andrievsky et al. (2011), and Bergemann et al. (2012a). For the Sr II resonance line, the NLTE abundance corrections are not large, typically within ±0.2 dex[2], *however, they are sensitive to variations of stellar parameters* (Bergemann et al. 2012a). Full 3D NLTE calculations for Sr have not yet been performed.

Using the NLTE technique presented in Bergemann et al. (2012a) we have now expanded the stellar sample in order to study the chemical evolution of Sr in the Galaxy. We derive NLTE Sr abundances, and NLTE stellar parameters for a sample of 21 stars plus comparison samples (François et al. 51 very metal-poor stars from 2007 and Bonifacio et al. 2009). We also include the predictions of the homogeneous chemical evolution model for the Galactic halo of Chiappini et al. (2008), computed with the most up-to-date Sr yields available in the literature. Given the still large uncertainties on the stellar yields, the goal of comparison between the data and the chemical evolution model is to give a first impression of how far or close the available stellar yields are from explaining the data. A comparison with inhomogeneous chemical evolution models, more suitable for low metallicity environments, is beyond the scope of the present paper, see Cescutti (2008); Cescutti & Chiappini (2010). The paper is structured as follows: Sect. 2 and 3 describe the observations, stellar parameters, and NLTE calculations, respectively. Section 4 and 5 present the results, yields, and the chemical evolution model. Conclusions can be found in Sect. 6.

2. Sample and data reduction

A sub-sample of stars (marked by 'u' in Sect. 4) was taken from Hansen et al. (2012). These stars have been observed with UVES/VLT (Dekker et al. 2000, $R \geq 40000$) between 2000 and 2002, and their spectra have been reduced with the UVES pipeline (v. 4.3.0). The spectra have a signal-to-noise ratio, S/N, > 100 at 3200 Å. Two stars (see 'h' in the following) have been observed with HIRES/Keck ($R \sim 60000$, Vogt et al. 1994). Their spectra are of similar quality as the UVES spectra, and they have been retrieved from the HIRES reduced data archive. The pipeline-reduced data were wavelength shifted, co-added and had their continua normalised before the analysis (for further details we refer to Hansen et al. 2012).

Three stars (HD 134169, HD 148816, HD 184448) were observed with the FOCES echelle spectrograph at the 2.2 m telescope of the CAHA observatory on Calar Alto, during 1999 and 2000, and were kindly made available to us by T. Gehren. The spectra have a resolution of ∼ 60000 and an S/N of ∼ 200 near 5000 Å. More details on the observations and data reduction can be found in Gehren et al. (2004, 2006).

We selected the stars according to the following criteria: 1) the observations cover the spectral range of the Sr I 4607 Å line, 2) accurate photometry is available, and 3) the stars cover a broad stellar parameter space to test the Sr I and Sr II abundance behaviour at different temperatures, gravities, and metallicities. Our sample thus consists of 21 dwarf, sub-giant, and giant stars. Here we have disregarded carbon enhanced metal-poor stars (CEMP-s/CEMP-no — with and without s-process overabundances). Since the CEMP-s stars tend to have very large s-process abundances, we are slightly biased against high Sr abundances at low metallicity.

For comparison, we include extremely metal-poor stars from François et al. (2007) and Bonifacio et al. (2009). For details about the observed data, we refer to these publications.

3. Methods

In this work, NLTE effects are accounted for in the determination of basic stellar parameters (surface gravity and metallicity) as well as Sr abundances. We describe the analysis in detail below.

3.1. Model atmospheres

All calculations in this work were performed with classical 1D LTE plane-parallel model atmospheres. We used the MAFAGS (Grupp 2004a,b) and MARCS (Gustafsson et al. 2008) models, which are both well-adapted for the analysis of late-type stars. The model atmosphere codes adopt slightly different prescriptions for the convective flux transport and background opacity. However, comparison of the model T(τ) relation showed that these differences are very small, and reveal themselves only in optically thick layers, where the treatment of convection is important (see Fig. 1). A comparison of the MAFAGS and MARCS models was presented in Bergemann et al. (2012b), where we showed that the differences in Fe abundances obtained with different model atmosphere codes are very small, typically within 0.05 dex. We further comment on this in Sect. 3.3.

3.2. Stellar parameters

Stellar parameters for the selected sample of stars were taken from (Hansen et al. 2012, 'H') and (Bergemann & Gehren 2008; Bergemann et al. 2012b, – 'BG';'B'), giving preference to parameters determined with IR photometry and parallaxes. The 'H', 'BG', and 'B' indicate the source of the temperature hereafter. A brief description of these data follows.

The effective temperatures were derived from several different colour indices and calibration methods (Alonso et al. 1996, 1999; Ramírez & Meléndez 2005; Masana et al. 2006; Önehag et al. 2009; Casagrande et al. 2010). We chose temperature calibrations that fall in the middle of the probed calibration ranges (see Hansen et al. 2012, for details). The reddening values were taken from Schlegel et al. (1998), and since all the reddening values are much smaller than 0.1 mag (Bonifacio et al. 2000), we have not applied their corrections to these values. Our chosen stellar parameters are also consistent with the effective temperatures ($T_{\rm eff}$) determined from the 1D fitting of Balmer profiles by Gehren et al. (2004, 2006). For the few stars (HD 19445, HD 142038, G 64-12) we have in common with Gehren et al.

[2] For very metal-poor (VMP; −3 < [Fe/H] < −2) stars the corrections are of the order of < ±0.08 and slightly larger for extremely metal-poor stars ([Fe/H] < −3).

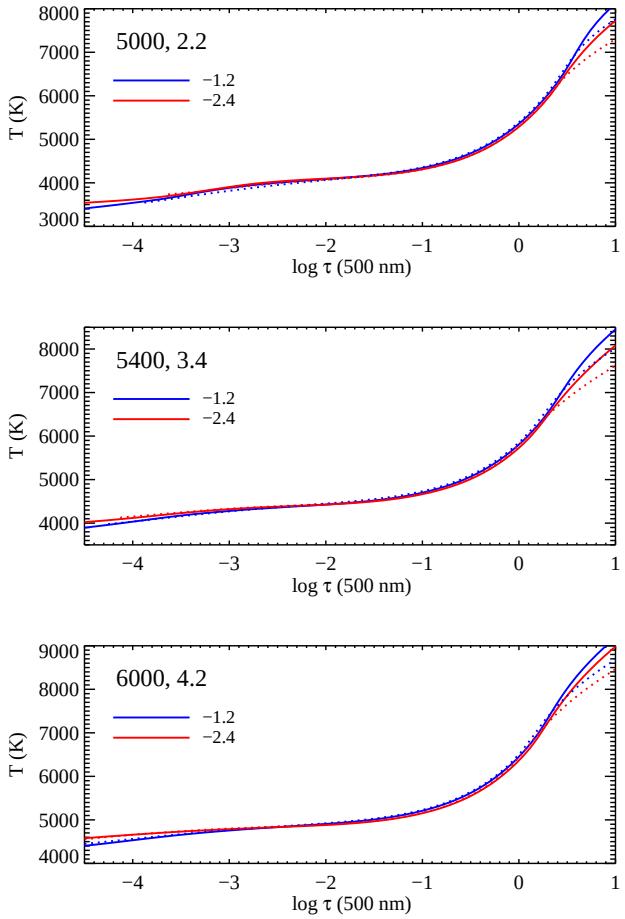

Fig. 1: Comparison of MARCS (dotted) and MAFAGS (solid) model atmospheres for selected stellar parameters at two different metallicities ([Fe/H] = −1.2, −2.4).

(2004, 2006), they derive $T_{\rm eff}$ = 5985, 5773, and 6407 K, respectively, with an *rms* offset of 10 K from our values. This confirms the agreement between the Balmer $T_{\rm eff}$ scale from Gehren et al. (2004, 2006) and the method described in Alonso et al. (1996) which we used here. Balmer line $T_{\rm eff}$'s (1D) from the same reference are in agreement with the values we adopted for HD 134169, HD 148816, HD 184448. The parameters for HD 122563 and G 64-12 are those from Bergemann et al. (2012b).

For the stars with parallax measurements, the surface gravity was calculated using the classical formula that relates mass, temperature, magnitude and parallax to gravity. Masses and bolometric corrections were taken from Nissen et al. (1997, 2002, 2007). Metallicities were then initially estimated in LTE and the effects of NLTE were taken into account by applying NLTE abundance corrections to Fe. These corrections were computed for the adopted Fe I line list by interpolation in the Fe NLTE grid presented by Lind et al. (2012). We note that for stars with metallicity [Fe/H] > −2, the systematic difference between LTE abundances of Fe I and Fe II is not large (≤ 0.1 dex). The Sr NLTE corrections also stay within 0.05 – 0.07 dex (see Sect. 4) consistent with the results in Bergemann et al. (2012a). The effect of NLTE becomes very important for Fe in very metal-poor stars with [Fe/H] < −2.5. In particular, most of the stars from our comparison samples (François et al. 2007; Bonifacio et al. 2009) are subject to NLTE metallicity corrections of the order +0.2 to +0.3 dex. For the extremely metal-poor (EMP; −4 < [Fe/H] < −3) giant stars, we obtain a maximum NLTE correction of $\Delta_{\rm NLTE}$[Fe/H] of +0.3 dex.

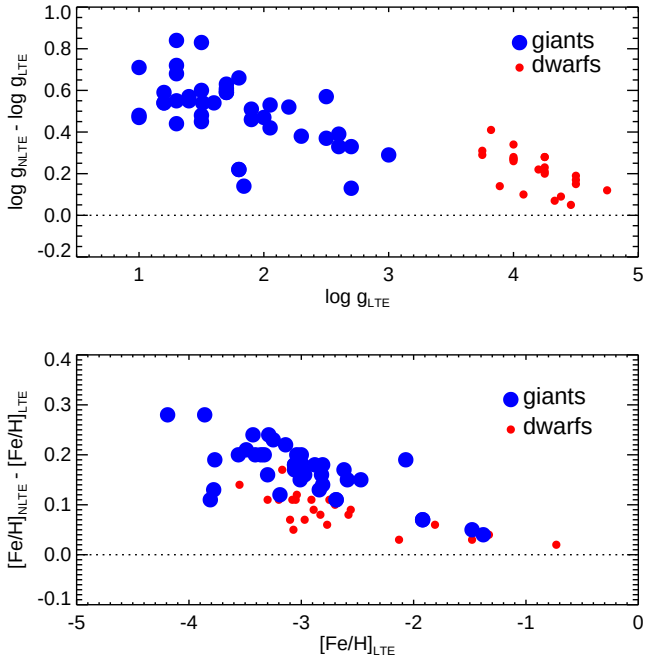

Fig. 2: Comparison of LTE and NLTE surface gravities (top) and metallicities (bottom).

For the other stars, without known parallaxes, the initial estimate of log g and [Fe/H] was obtained from the LTE ionization equilibrium of Fe, and Fe NLTE corrections were applied to both gravity and metallicity. To compute the NLTE correction for surface gravity, we used the approximate $\Delta_{\rm NLTE}$ log g - $\Delta_{\rm NLTE}$[Fe/H] calculations from Lind et al. (2012, their Sect. 3). The changes in log g due to NLTE effects are significant and have a clear effect on the [Sr/Fe] ratios derived from the gravity-sensitive Sr II lines, compared to the changes in metallicity. The NLTE gravity corrections reach up to ∼ +0.8 dex for the most metal-poor giants in our sample. The influence of $T_{\rm eff}$ on Sr II is minor. By changing the temperature with its uncertainty, the Sr II abundance changes by 0.01-0.05 dex, while the change in Sr I is much larger (see Sect. 4.1). The NLTE and LTE stellar parameters are compared in Fig. 2.

As seen from Fig. 3 the temperatures for seven stars taken from three different sources (Casagrande et al. 2010; Bergemann et al. 2012a; Hansen et al. 2012) agree within 40 K in most cases, and for a few stars (e.g. HD106038) the difference between the two IRFM methods (Alonso et al. 1996; Casagrande et al. 2010) is 170 K. This difference is within the combined errors, if we include systematic errors as well as the uncertainty on $E(B-V)$. The dwarfs from the comparison sample (Bonifacio et al. 2009) had their temperatures estimated from Hα line profile fitting, which yielded values in good agreement with those determined from Alonso et al. (1996) calibrations. We refer the reader to Bonifacio et al. (2009) and Sbordone et al. (2010) for further details on Hα line profile fitting. The giants from the second comparison sample (François et al. 2007) had their temperatures determined by the use of broad range photometry calibrations from

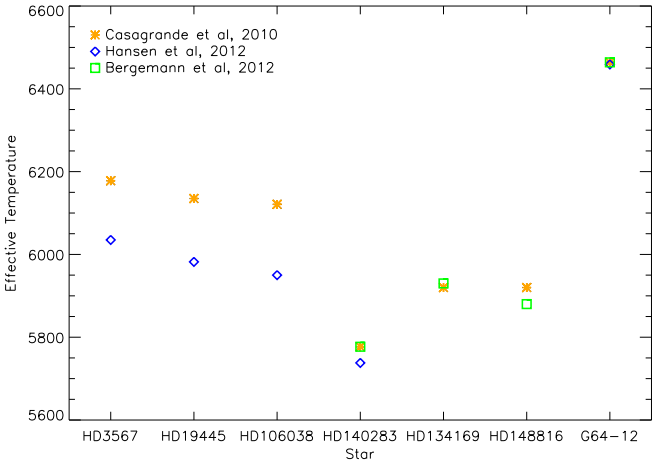

Fig. 3: Comparison of effective temperatures determined with different methods for seven stars. The legend indicates the original paper (Casagrande et al. 2010; Hansen et al. 2012; Bergemann et al. 2012a, – yellow '*', blue diamond, and green square, respectively) from which the temperatures have been taken.

Alonso et al. (1999). This is the same method we applied here, and the differences/offsets between our temperature determinations and those made for the comparison samples are minimal.

The microturbulence velocity was fixed by requiring that Fe I lines yield the same abundances regardless of their equivalent width. In our parameter space, the NLTE corrections to microturbulence (Lind et al. 2012) are smaller than the formal uncertainty of ξ_t (±0.15 km/s) and were not considered here.

The main error in our photometric temperatures comes from reddening ($\lesssim$ ±0.05 mag). For Balmer lines, the temperature error is largely internal and is determined from the profile fitting (this applies to the six stars marked by a 'B' in the following). The error in the adopted $\log g$ values is dominated by that of parallaxes ($\lesssim$ ±1.0"). The errors in [Fe/H] and microturbulence are assumed to be 0.1(5) dex and 0.15 km/s, respectively. After propagating all stellar parameter uncertainties, we adopted a common set of uncertainties for our stars of ($T_{\rm eff}$/$\log g$/[Fe/H]/ξ): ±100 K/0.2 dex/0.1 dex/0.15 km/s. For the most metal-poor stars, we find slightly larger values: ±100 K/0.25 dex/0.15 dex/0.15 km/s. These errors are internal to our method. *The differences between LTE and NLTE stellar parameters highlights that systematic errors in LTE are larger than the internal errors.*

3.3. Sr abundance determinations

The NLTE statistical equilibrium calculations for Sr are performed with the revised version of the DETAIL code (Butler & Giddings 1985). The new model atom of Sr and other related aspects of the NLTE calculations are described in detail in Bergemann et al. 2012a. The NLTE effects on the Sr I lines are primarily caused by over-ionisation, which leads to systematically higher NLTE abundances compared with LTE, especially for more metal-poor and hotter stars. In contrast, deviations from LTE in the Sr II lines are largely driven by strong line scattering. As a consequence, the differences between the LTE and NLTE abundances may be positive or negative, depending on temperature, gravity, and metallicity of a star.

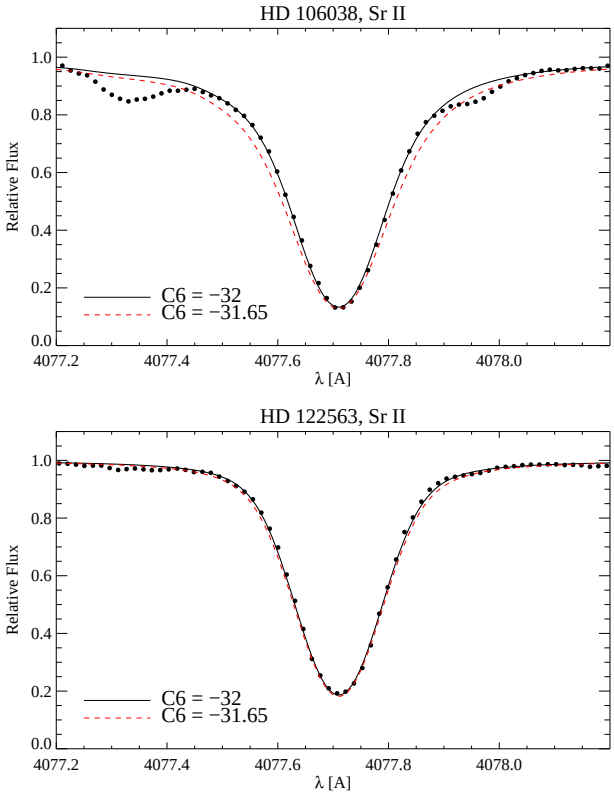

Fig. 4: Effect of elastic H I collisions on the 4077 Å lines expressed through different C_6 values (red dashed and black solid line) - compared to observations (black dots) of a dwarf (HD 106038) and a metal-poor giant (HD 122563) star.

The LTE and NLTE abundances of Sr in the selected metal-poor stars are determined as follows. The LTE abundances are synthesised with MOOG, while NLTE synthesised abundances are derived using the SIU code (Reetz 1999), where the NLTE departure coefficients are computed with DETAIL. In both cases we apply the same atomic data. We note that the LTE abundances from SIU and MOOG agree within 0.1 dex. This difference is a combination of local continuum placement (which can be up to 0.05 dex when set locally by eye) and due to the different synthesis codes, since the model atmospheres are very similar, as seen from Fig. 1, they almost do not contribute to this difference. Only very deep in the atmosphere (close to $\tau = 1$) do the MARCS and MAFAGS models differ due to a more efficient transport of convective flux in the MARCS models, which leads to a cooler atmosphere compared to MAFAGS. For 18 stars, with a four star overlap with the SIU analysis, we first determine LTE abundances by spectrum synthesis with the MOOG code. To obtain NLTE abundances, we then apply the NLTE corrections calculated with DETAIL and MAFAGS. We do not perform differential abundance analysis with respect to the Sun.

In particular, to remain consistent with our previous analysis, we use the van der Waals broadening and gf-values from Bergemann et al. (2012a) (see Table 1). According to this study the damping constants for the Sr II lines could be somewhat uncertain. Variation of $\log C_6$ by ±0.35 (~ 20%) leads to a change of abundances by ∓0.15 dex for the 4077Å Sr II line in the metal-poor stars with [Fe/H]> −1.5 (see Fig. 4), but has only minor effect at very low metallicity (~ ∓0.05 dex). The accuracy of the gf-value for the 4607 Å Sr I line was critically evaluated by

Table 1: Atomic data for Sr I and II

Element	λ Å	χ eV	loggf	log(γ/N$_H$) rad cm^3 s^{-1}	log C$_6$ cm^6 s^{-1}
Sr I	4607.33	0.0	0.283	-7.53	-31.2
Sr II	4077.71	0.0	0.158*	-7.81	-32.0

Notes. (*) Total log gf value. Further details and hfs splitting can be found in Bergemann et al. (2012a).

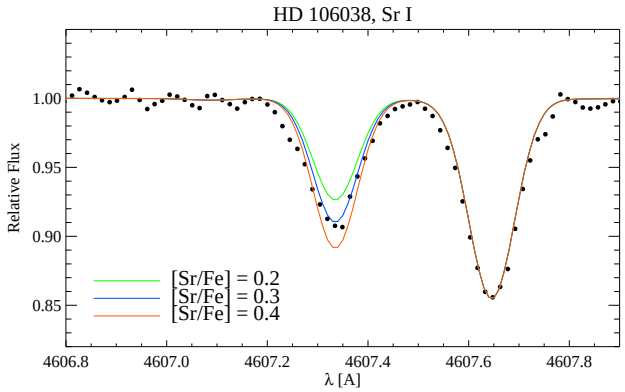

Fig. 5: Synthetic spectra (solid lines) of the 4607 Å Sr I line plotted on top of the observed spectrum of HD 106038 (dots).

the NIST database. The uncertainties are less than one percent and yield accurate abundances even for metal-rich stars (see Fig. 5), whereas the Sr II resonance lines at 4077 and 4215 Å are too blended and strong to give any reliable information about the solar Sr abundance (see Fig. 6). We derive our Sr I abundances from the 4607 Å line and the Sr II abundances from the 4077 Å line, since all our stars have sub-solar metallicities.

We test the *Abfind* package in MOOG, which uses the measured equivalent widths (EW) to compute abundance by the curve-of-growth method. We find, however, that this method yields abundances in slight disagreement (±0.04 < [Sr/Fe]$_{\rm EW-syn}$ < ±0.25) with the results obtained by the full profile fitting using the *Synth* (synthesis) package of the same code (see the online material). Depending on the line properties, in particular equivalent width, the abundance is either over- or under-estimated (Table 2). This is not unexpected; the Sr I line is very weak in metal-poor stars, and both Sr II lines are strong, damping sensitive, and affected by blends. For example, the EWs determined by fitting Voigt and Gaussian profiles in IRAF ('/' separated entries in the 'EW' columns in Table 2) differ generally by 5–10% (in a few cases like the VMP dwarf HD 106038 the difference is approximately a factor of three larger). As a result, abundances derived using the EWs may be discrepant by up to 0.4 dex (Fig. 7). However, except from one case (the EMP subgiant HD 140283), the largest difference between EW and synthesis determined abundances are on the order of ±0.1 dex (see online material). This value might be slightly overestimated due to local continuum placement.

Blends influence abundance determinations both in the metal-poor and metal-rich part of our sample. Features in the blue and red wings of the 4077 Sr II line, ~ 0.3 Å away from the line center, vanish only in the spectra of most metal-poor stars, [Fe/H] < −2. These blends are due to lanthanum, chromium and dysprosium. The Sr II line at 4215 Å is blended by the two Fe I

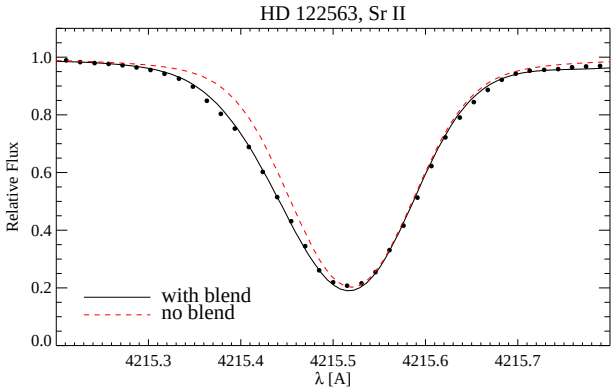

Fig. 6: Comparison of synthetic profiles (lines) of the Sr II line to observations of HD122563 (black dots). The syntheses have been computed with (black solid line) and without (red dashed line) the Fe I blends for the 4215 Å Sr II line.

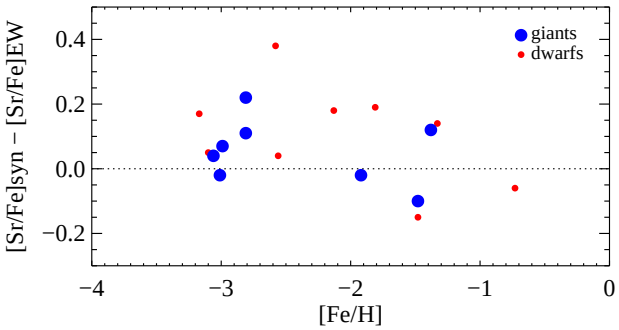

Fig. 7: Difference in Sr abundances between EW and synthesis. Dwarfs/giants are shown as small red/big blue filled circles, respectively.

lines at 4215.42 and 4216.18 Å. The former is rather strong and clearly distorts the shape of the Sr II profile, as directly seen in the very high-resolution spectra. Figure 6 shows that even for the very metal-poor giant HD 122563 with [Fe/H]$_{\rm NLTE}$ = −2.5, the abundance is over-estimated by 0.14 dex (when synthesised) if this blend is not taken into account. Therefore, the abundance determined from the 4215 Å Sr II line is subject to a systematic uncertainty, and the blend is sensitive to $T_{\rm eff}$, log g, and metallicity.

On these grounds, we do not include the 4215 Å Sr II line in the abundance calculations. Furthermore, for the comparison samples from François et al. (2007) and Bonifacio et al. (2009) only measurements for the 4077 Å Sr II line are available. Hence, for the sake of consistency and to retain the full sample size, we only use the 4077 Sr II line.

The Sr I line is generally weak, and regardless of the profile fitted to this line, the EW-converted abundances tend to be larger than the synthesised abundances. This might be due to an iron blend in the red wing of this neutral strontium line (see Fig. 5, where a stronger Fe line is blending into the red wing of the Sr I line).

The LTE abundances derived for our sample have been calculated with LTE stellar parameters (as described in Sect. 3.2) using the 1D LTE synthetic spectrum code MOOG to synthesise spectra for these stars. The EWs for the dwarf comparison sam-

Table 2: Example of LTE [Sr/Fe] abundances for a dwarf, sub-giant, and giant from the measured equivalent widths (EW) and from synthesis (synt). The measured Gauss/Voigt EWs (G/V) are given in mÅ together with the stellar parameters.

Star	4077 EW	EW G/V [mÅ]	4077 synt	4607 EW	EW G/V [mÅ]	4607 synt	$T_{\rm eff}$ [K]	$\log g$	$[{\rm Fe/H}]_{LTE}$	ξ [km/s]
HD106038	0.28/0.65	186.1/271.0	0.5	0.43/0.47	13.1/14.1	0.33	5950	4.33	−1.48	1.1
HD140283	−0.44/ − 0.33	75.8/79.8	−0.15	–	–	–	5777	3.70	−2.58	1.5
HD122563	−0.34/ − 0.09*	158.8/184.0	−0.05	−0.54*	2.9	< −0.6	4665	1.65	−2.50	1.8

Notes. (*) Value uncertain

ple have been taken from Bonifacio et al. (2009). We measured the EWs for the remaining stars. The LTE Sr II abundances for the comparison samples (dwarfs and giants) have been redetermined with MARCS models and MOOG, using the solar abundance, from Anders & Grevesse (1989), which we have adopted for this study. The LTE abundances we calculated agree within 0.05 - 0.1 dex with those published in (François et al. 2007, F07) and (Bonifacio et al. 2009, B09), and only for a handful of stars is the difference greater than 0.2 dex.

The correction for NLTE effects is most conveniently performed by differentiating LTE and NLTE curves-of-growth at a given line strength. The method we have adopted thus relies on the determination of EWs and subsequent translation to LTE and NLTE abundances. From the comparison sample (the *"First Stars"* samples) we only have these EWs. When determining EWs by profile fitting with a single component, unresolved blends may play a role, and hence we have derived both LTE and NLTE EW-based abundances and compare them to synthesised abundances in order to assess the impact the single-line assumption have on the final abundances. For all the tests related to atomic data, blends and profile fitting, we have maintained one set of stellar parameters for each star (those listed in Table 3). Thus, the resulting difference in abundance is an expression of uncertainties in the atomic data, unknown blends and continuum placement.

From Fig. 7 we estimate that the Sr abundances from the metal-rich stars might be overestimated when using the EW method, while Sr in the metal-poor stars will be overestimated with < 0.32 dex. Another part of the over-/under-estimation can be assigned to the line profile fitting and continuum placement.

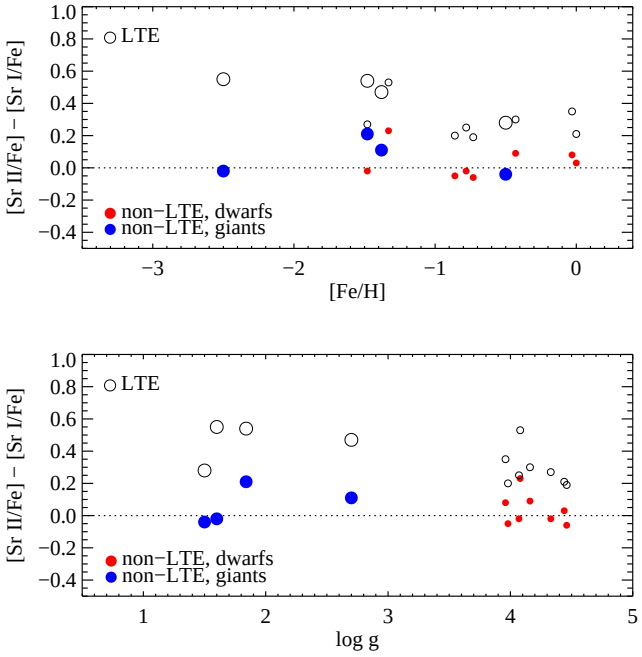

Fig. 8: Sr LTE (open circles) and NLTE abundance differences (filled big blue/small red circles for giants/dwarfs) as a function of [Fe/H] (top panel) and $\log g$ (bottom panel).

4. Results: LTE vs NLTE

The results for our sample are summarised in Table 3, which provides the mean of synthesised abundances for Sr I and Sr II. Their differences are shown in Fig. 8 as a function of stellar [Fe/H] and $\log g$. The LTE and NLTE line by line abundances from both EW and synthesis are also given in online Table A.1 (for our sample).

The LTE approximation fails to establish ionisation balance of Sr I and Sr II. Fig. 8 shows that the offset between the two ionisation stages is about 0.2 dex for dwarfs, but it increases up to 0.5 dex for giants. This difference is mainly caused by the progressively increasing systematic error in the LTE abundance inferred from the Sr I line, which shows NLTE abundance corrections of up to 0.5 dex at low metallicity and low gravity (online Table A.1). Although the NLTE effects on the resonance Sr II lines are not significantly pronounced, they depend on stellar parameters, particularly on the [Fe/H], or, equivalently, the Sr abundance itself (see discussion in Sect. 3.3). In Table 3, we see that the LTE abundances obtained from the Sr II lines can be over- or underestimated by up to 0.1 dex, which may introduce a spurious systematic trend, or, more likely give rise to a larger line-to-line scatter. For our stellar sample, even though the line-to-line scatter is clearly smaller under NLTE, the star-to-star scatter almost remains the same under both LTE and NLTE. The results for the comparison samples (*'First Stars'* – F07, and B09) are shown in Table 4.

Figure 9 shows the [Sr/Fe] ratios as a function of [Fe/H]. In the figure, the error bars are the total, propagated uncertainties, computed as described below. The exceptions are HD 3567, HD 19445, HD 122563, and HD126587 with upper limits on the abundance from the 4607 Å Sr I line.

4.1. Uncertainties

A number of test calculations varying the input parameters in the spectrum synthesis were performed for the two representative stars with the same metallicity: HD 106038 (dwarf) and HD 74462 (giant). In particular, we are interested in the sensitivity of the abundances to the model atmosphere parameters: $T_{\rm eff}$, $\log g$, [Fe/H], and microturbulence (Table 5). As seen from this table, the Sr II line at 4077 Å is very strong and mainly sensitive to $\log g$

Table 3: Stellar parameters and the derived Sr abundances ± the standard deviation for the selected sample of stars. A (1) indicates that the Sr abundance is derived only from the 4077Å Sr II line. The subscript tells if the parameter has been corrected for NLTE effects. If the gravities are derived from parallaxes their values will be the same in both cases, however, when derived from ionisation equilibrium the NLTE corrected $\log g_{corr.}$ will differ from the LTE Fe I based $\log g$. All LTE abundances have been derived in MOOG, except from the stars with an 's' superscript, they have had their abundances derived in SIU.

Star	$\pi \pm \sigma$ [mas]	T_{eff} [K]	$\log g$	$\log g_{corr.}$	$[Fe/H]_{LTE}$	$[Fe/H]_{NLTE}$	ξ km/s	$[Sr/Fe]_{LTE}$	$[Sr/Fe]_{NLTE}$	Comment
HD 3567	9.57±1.38	6035	4.08	4.08	−1.33	−1.29	1.5	-0.03 ± 0.8^{x}	0.06 ± 0.8^{x}	[u,H]
HD 19445	25.85±1.14	5982	4.38	4.38	−2.13	−2.10	1.4	0.13 ± 0.8^{x}	0.16 ± 0.8^{x}	[u,H]
HD 106038	9.16±1.50	5950	4.33	4.33	−1.48	−1.45	1.1	0.42±0.12	0.45 ± 0.21	[u,H]
HD 121004	16.73±1.35	5711	4.46	4.46	−0.73	−0.71	0.7	0.18 ± 0.04	0.26 ± 0.17	[u,H]
HD 122196	9.77±1.32	6048	3.89	3.89	−1.81	−1.75	1.2	$0.24^{(1)}$	$0.19^{(1)}$	[u,H]
HD 134169	16.80±1.11	5930	3.98	3.98	—	−0.86	1.8	−0.05 ± 0.14	−0.06 ± 0.13	[f,s,BG]
HD 140283	17.16±0.68	5777	3.70	3.70	−2.58	−2.38	1.5	$-0.15^{(1)}$	$-0.37^{(1)}$	[u,H,B]
HD 148816	24.34±0.90	5880	4.07	4.07	—	−0.78	1.2	−0.13 ± 0.18	−0.13 ± 0.17	[f,s,BG]
HD 184448	19.16±0.63	5765	4.16	4.16	—	−0.43	1.2	0.00 ± 0.21	−0.01 ± 0.21	[f,s,BG]
G 64-12	0.57±2.83	6464	4.30	4.30	−3.24	−3.12	1.5	$0.00^{(1)}$	$0.17^{(1)}$	[u,B]
G 64-37	2.88±3.10	6494	3.82^{*}	4.23	−3.17	−3.00	1.4	$0.08^{(1)}$	$0.17^{(1)}$	[u,H]
HD 122563	4.22±0.35	4665	1.65	1.65	−2.60	−2.50	1.8	-0.23 ± 0.8^{x}	-0.12 ± 0.8^{x}	[u,B]
HD 175305	6.18±0.56	5100	2.70	2.70	−1.38	−1.34	1.2	−0.12 ± 0.32	0.04 ± 0.1	[h,H]
BD -133442	–	6450	4.20	4.42	−2.56	−2.47	1.5	$0.30^{(1)}$	$0.21^{(1)}$	[u,H]
CS 30312-059	–	5021	1.90	2.41	−3.06	−2.89	1.5	$0.50^{(1)}$	$0.31^{(1)}$	[h,H]
CS 31082-001	–	4925	1.51	2.05	−2.81	−2.63	1.4	$0.70^{(1)}$	$0.60^{(1)}$	[h,H]
HD 74462	–	4590	1.84	1.98	−1.48	−1.43	1.1	−0.25 ± 0.35	−0.14 ± 0.03	[h,H]
HD 126238	–	4900	1.80	2.02	−1.92	−1.85	1.5	−0.17 ± 0.24	0.01 ± 0.06	[u,H]
HD 126587	–	4950	1.90	2.36	−3.01	−2.86	1.65	0.23 ± 0.8^{x}	0.22 ± 0.8^{x}	[u,H]
HE 0315+0000	–	5050	2.05	2.47	−2.81	−2.67	1.7	$0.39^{(1)}$	$0.23^{(1)}$	[u,H]
HE 1219-0312	–	5100	2.05	2.58	−2.99	−2.81	1.65	$0.29^{(1)}$	$0.12^{(1)}$	[u,H]

Notes. $^{(*)}$ Value from ionisation equilibrium
$^{(x)}$ Weighted average, which includes an upper limit that was given half weight. The large uncertainty is a reciprocal square root of the summed weights.
$^{(u,f,h)}$ Observed spectra from: ^{u} UVES/VLT, ^{f} FOCES/Calar-Alto Gehren et al. (2004, 2006), ^{h} HIRES/Keck
$^{(B,BG,H)}$ Temperature from (Bergemann et al. 2012b, B), (Bergemann & Gehren 2008, BG), and (Hansen et al. 2012, H), respectively.

and ξ. In comparison, the neutral Sr abundance from the weaker 4607 Å line is seen to be temperature and [Fe/H] sensitive, but almost not affected by $\log g$ and ξ.

Several of the Sr I abundances presented in online Table A.1 are only upper limits, which is why we applied a weighted average and a corresponding reciprocal square root of the summed weights (see Taylor 1997). The final [Sr/Fe] abundances and their uncertainties are shown in Table 3. The upper limits of Sr I were given half the weight of Sr II. This overestimates the uncertainty a bit. However, with only two measurements this approach seems sensible. In some stars only Sr II could be measured, hence the abundance is based on one trustworthy line only. To estimate the uncertainty in this case we have made independent measurements of the 4077 Sr II line, and found the derived abundances to be consistent to within 0.0 - 0.1 dex. An average value of ±0.05 dex was adopted instead of the standard deviation otherwise applied for the stars with two detectable lines.

We summarise that the assumption of LTE especially in metal-poor, low gravity stars will, in addition to not fulfilling Sr ionisation balance, also introduce a weak spurious trend of Sr abundances with metallicity. The Sr I resonance line would consistently under-estimate the Sr abundance trend, whereas the abundances obtained from the subordinate Sr II lines would be systematically too large by ∼ 0.05 dex. Whereas the abundances derived from the Sr I line are significantly affected by NLTE line formation, Sr II lines are less so. However, NLTE effects for Fe must be accounted for in the spectroscopic gravity determination in order to derive accurate abundances for Sr II lines. *Furthermore, we note that the large star-to-star scatter found in LTE abundance studies remains under NLTE even at extremely low metallicities.*

Table 5: Uncertainties in the individual LTE Sr I and II abundances in a giant (HD 74462) and a dwarf (HD 106038) star.

HD 74462: [Sr/Fe]	0.1	-0.5
Parameter/line [Å]	4077	4607
T ±100	±0.03	±0.17
logg ±0.2	±0.04	±0.01
[Fe/H] ± 0.1	±0.12	±0.09
ξ ± 0.15	±0.07	±0.01
Propagated uncertainty	±0.15	±0.19
HD 106038: [Sr/Fe]	0.65	0.33
T ±100	±0.04	±0.09
logg ±0.2	±0.17	±0.01
[Fe/H] ± 0.1	±0.22	±0.09
ξ ± 0.15	±0.13	±0.01
Propagated uncertainty	±0.3	±0.13

Our analysis of the chemical evolution of Sr in NLTE is different from previous studies. Andrievsky et al. (2009) already performed NLTE calculations for Sr, however, their stellar parameters were determined assuming LTE. These have a measurable impact on the Sr abundances. The difference in the overall

Table 4: Basic parameters and the EW calculated Sr abundances from the 4077Å line for the comparison stars. The top part contains dwarf stars from the comparison sample, while the lower part shows the giants from the second comparison sample. Details and subscripts are described in Table 3.

Star	T_{eff} [K]	$\log g$	$\log g_{corrected}$	$[Fe/H]_{LTE}$	$[Fe/H]_{NLTE}$	ξ [km/s]	$[Sr/Fe]_{LTE}$	$[Sr/Fe]_{NLTE}$
Dwarf sample^{FS,B09}								
BS16023-046	6364	4.50	4.69	−2.97	−2.90	1.3	−0.20	−0.17
BS16076-006	5199	3.00	3.29	−3.81	−3.70	1.4	0.67	-0.64
BS16968-061	6035	3.75	4.04	−3.05	−2.94	1.5	−1.59	−1.58
BS17570-063	6242	4.75	4.87	−2.92	−2.87	0.5	0.03	−0.02
CS22177-009	6257	4.50	4.67	−3.10	−3.03	1.2	−0.15	−0.12
CS22888-031	6151	5.00	5.09	−3.30	−3.26	0.5	0.05	0.09
CS22948-093	6356	4.25	4.53	−3.30	−3.19	1.2	−0.08	−0.01
CS22953-037	6364	4.25	4.48	−2.89	−2.80	1.4	−0.45	−0.46
CS22965-054	6089	3.75	4.06	−3.04	−2.92	1.4	−2.09	−2.17
CS22966-011	6204	4.75	4.87	−3.07	−3.02	1.1	0.88	0.95
CS29499-060	6318	4.00	4.26	−2.70	−2.60	1.5	−0.63	−0.70
CS29506-007	6273	4.00	4.27	−2.91	−2.80	1.7	−0.49	−0.50
CS29506-090	6303	4.25	4.46	−2.83	−2.75	1.4	0.33	0.27
CS29518-020	6242	4.50	4.65	−2.77	−2.71	1.7	0.08	0.05
CS29518-043	6432	4.25	4.53	−3.20	−3.09	1.3	—	—
CS29527-015	6242	4.00	4.34	−3.55	−3.41	1.6	0.12	0.22
CS30301-024	6334	4.00	4.27	−2.75	−2.64	1.6	−0.41	−0.47
CS30339-069	6242	4.00	4.28	−3.08	−2.97	1.3	0.43	0.40
CS31061-032	6409	4.25	4.45	−2.58	−2.50	1.4	−0.48	−0.54
Giant sample^{FS,F07}								
BD+17:3248	5250	1.40	1.97	−2.07	−1.88	1.5	0.00	−0.09
BD-18:5550	4750	1.40	1.95	−3.06	−2.88	1.8	−1.03	−1.12
BS16467-062	5200	2.50	3.07	−3.77	−3.58	1.6	−1.96	−1.99
BS16477-003	4900	1.70	2.29	−3.36	−3.16	1.8	0.06	−0.19
BS17569-049	4700	1.20	1.74	−2.88	−2.70	1.9	0.17	−0.18
CD-38:245	4800	1.50	2.33	−4.19	−3.91	2.2	−0.72	−0.82
CS22169-035	4700	1.20	1.79	−3.04	−2.84	2.2	-0.33	−0.30
CS22172-002	4800	1.30	2.14	−3.86	−3.58	2.2	−1.40	−1.60
CS22186-025	4900	1.50	2.10	−3.00	−2.80	2.0	0.61	0.41
CS22189-009	4900	1.70	2.33	−3.49	−3.28	1.9	−1.01	−1.07
CS22873-055	4550	1.00	1.48	−2.99	−2.83	2.2	−0.16	−0.30
CS22873-166	4550	1.00	1.47	−2.97	−2.81	2.1	0.07	−0.07
CS22878-101	4800	1.30	1.98	−3.25	−3.02	2.0	−0.41	−0.36
CS22885-096	5050	2.60	2.99	−3.78	−3.65	1.8	−1.44	−1.47
CS22891-209	4700	1.00	1.71	−3.29	−3.05	2.1	0.15	−0.01
CS22892-052	4850	1.60	2.14	−3.03	−2.85	1.9	0.41	0.20
CS22896-154	5250	2.70	3.03	−2.69	−2.58	1.2	0.32	0.18
CS22897-008	4900	1.70	2.30	−3.41	−3.21	2.0	−0.39	−1.20
CS22948-066	5100	1.80	2.46	−3.14	−2.92	2.0	0.46	0.25
CS22952-015	4800	1.30	2.02	−3.43	−3.19	2.1	−0.96	−1.07
CS22953-003	5100	2.30	2.68	−2.84	−2.71	1.7	0.13	−0.01
CS22956-050	4900	1.70	2.29	−3.33	−3.13	1.8	−0.47	−0.42
CS22966-057	5300	2.20	2.72	−2.62	−2.45	1.4	−0.33	−0.44
CS22968-014	4850	1.70	2.31	−3.56	−3.36	1.9	−1.81	−1.69
CS29491-053	4700	1.30	1.85	−3.04	−2.86	2.0	−0.15	−0.36
CS29495-041	4800	1.50	1.98	−2.82	−2.66	1.8	−0.23	−0.36
CS29502-042	5100	2.50	2.87	−3.19	−3.07	1.5	−1.99	−2.05
CS29516-024	4650	1.20	1.74	−3.06	−2.88	1.7	−0.47	−0.61
CS29518-051	5200	2.60	2.93	−2.69	−2.58	1.4	0.06	−0.07
CS30325-094	4950	2.00	2.47	−3.30	−3.14	1.5	−2.38	−2.47
HD2796	4950	1.50	1.95	−2.47	−2.32	2.1	−0.23	−0.24
HD186478	4700	1.30	1.74	−2.59	−2.44	2.0	0.05	−0.12

Notes. $^{(FS)}$ The synthesised LTE abundances can be found in the *First Stars* papers; Dwarfs from Bonifacio et al. (2009, B09), and giants from François et al. (2007, F07)

trend of [Sr/Fe] with metallicity (Bergemann et al. (2012a), and our Fig. 9) is detectable, and is best seen in Fig. 10. As discussed in Bergemann et al. (2012a), the model atom by Andrievsky et al. (2011) is less complete compared to ours, and we incorporated new atomic data, which influences the magnitude of NLTE abundance corrections. For the resonance Sr II line at 4077 Å, our

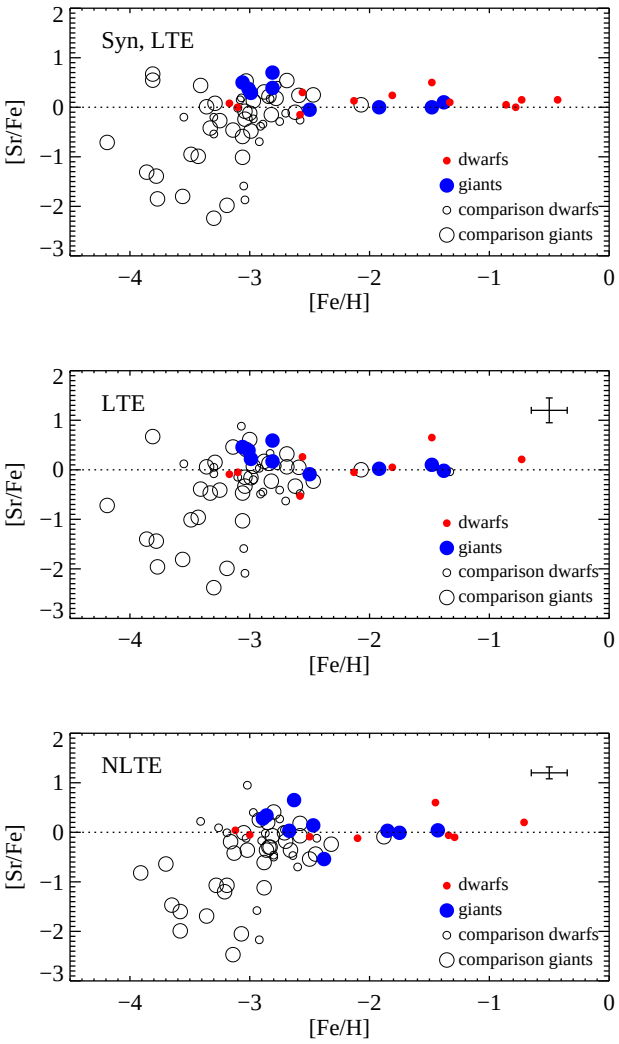

Fig. 9: Upper figure: LTE Sr synthesised (Syn) abundances for F07, B09 (open circles), and our sample (filled circles - giants big, blue and dwarfs small, red). The figure in the middle shows the EW-based abundances for the same stars. Lower figure: The same samples but with NLTE corrected stellar parameters, and NLTE corrected EW-based Sr abundances.

NLTE corrections are mildly negative for any $\log g$ and T_{eff} at [Fe/H] = −3, whereas Andrievsky et al. (2011) obtain large positive corrections for dwarfs and negative ΔNLTE for giants.

5. Discussion — Chemical evolution of Sr

Since we wish to assess the impact of the LTE assumption vs NLTE on the chemical evolution of Sr, we have selected a handful of Sr yields, covering both s- and r-process contributions. We probe how LTE vs NLTE abundances behave in a Galactic chemical evolution scheme. The yields will briefly be outlined below.

5.1. Theoretical predictions of stellar Sr yields

Here we consider the weak r-process yields from Arcones & Montes (2011) and Wanajo et al. (2010), and the s-process yields from Bisterzo et al. (2010), Frischknecht et al. (2012), and our own AGB yields based on the calculations presented in Karakas et al. (2012) and Lugaro et al. (2012) that extend down to low metallicities of [Fe/H] = -2.3.

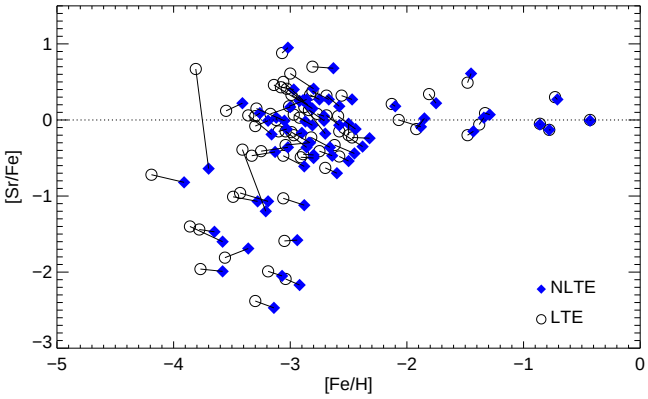

Fig. 10: Difference in [Sr/Fe] ratios between NLTE (blue diamonds) and LTE (open circles).

The yields from Wanajo et al. (2010) describe the ejecta from low-mass ($\sim 9 M_\odot$) faint core-collapse electron-capture supernovae (ECSN). These may occur frequently even at low metallicity, and their yields can therefore not be neglected when considering the evolution of Sr. The amount of Sr injected into the interstellar medium (ISM) can for a low entropy (13-15 k_B/baryon) vary between $1.78 \cdot 10^{-4} M_\odot$ (referred to as *high yield* in Sect. 5.2) for an electron fraction (Y_e) of 0.4, reaching a maximum at $Y_e = 0.3$ ($5.69 \cdot 10^{-4} M_\odot$ — *standard yield*), and declining fast to a minimum Sr yield of $1.62 \cdot 10^{-9} M_\odot$ (referred to as *low yield*), which is obtained with $Y_e = 0.15$. The Y_e-interval is adopted from the model-to-observation comparison made in Hansen et al. (2012). Low Y_e values are expected in low-mass progenitors due to their fast explosions. Small bubbles expand fast enough to inhibit the neutrino to increase the electron fraction.

Neutrino-driven winds following immediately after supernova explosions, also from more massive progenitors, will also provide a contribution to the amount of Sr in the ISM. The wind predictions we have incorporated here, are based on the computations presented in Arcones & Montes (2011). Here we have tested the impact that wind parameters, such as entropy, electron fraction, and expansion time scale, have on the neutron-capture nucleosynthesis in the wind. The effect of progenitor mass and progenitor metallicity remains an open question, since the supernova models still have too large uncertainties to constrain these quantities. Nonetheless, we note that since this process is a primary process the impact of metallicity is not the most important factor when trying to constrain the yields. Now, assuming a neutron-rich wind with the electron fraction constricted to $0.4 < Y_e < 0.49$ (as currently suggested by Martínez-Pinedo et al. 2012; Roberts & Reddy 2012; Roberts 2012), we can try to loosely confine some parameters to realistic ranges by setting an entropy interval of 50 to 150 k_B/baryon, and a wind expansion time scale limited to a few milliseconds. These are typical values found in hydrodynamical wind simulations (Arcones et al. 2007; Fischer et al. 2010) and lead to Sr yields spanning 10^{-4} – 10^{-7} $M_\odot$, where the largest contribution comes from 12 – 25 $M_\odot$ supernovae, and the smallest yield could be assigned to 8 – 12 $M_\odot$ SN explosions. Generally speaking, the smaller Sr yields can be assigned to low-mass progenitors, while more massive ones produce larger Sr yields.

The first s-process yield we consider here are those of Bisterzo et al. (2010), who provide the yields from AGB stars in the mass range $1.3 - 2M_{\odot}$ at different metallicities ([Fe/H]): 0, -0.8, -1.6, and -2.6 (S. Bisterzo, priv. comm.). These yields have been calculated with the FRANEC (Frascati Phapson-Newton Evolutionary Code) that uses reaction rates from the KADoNiS and NACRE databases. The neutron-capture elements are created in ^{13}C pockets and brought to the stellar surface during thermal pulses. The AGB star experiences a mass loss on the order of $10^{-4} - 10^{-7} M_{\odot}/yr$ where the interval between successive thermal pulses lasts for about $10^4 - 10^5$ years depending on the AGB core mass (e.g., see model data published in Karakas et al. 2012 or Cristallo et al. 2011). The impact at low metallicity ([Fe/H]< -2.6), which we are interested in, is minor and would need to be extrapolated. However, yields from low mass AGB stars are important at higher metallicities.

We also use AGB yields based on the nucleosynthesis calculations presented in Karakas et al. (2012) and Lugaro et al. (2012). These calculations use reaction rates from the NACRE and JINA databases, which includes the KADoNIS neutron-capture cross sections. In comparison to the yields from Bisterzo et al. 2010, these span a range from $0.9M_{\odot}$ to $6M_{\odot}$ at [Fe/H] = -2.3; at higher metallicities we span a mass range from $1.25M_{\odot}$ to $6M_{\odot}$ at [Fe/H] = -0.15 and $5M_{\odot}$ to $8M_{\odot}$ at [Fe/H] = +0.14 (slightly super solar). For the heaviest of these stars, the main neutron source is the ^{22}Ne(α,n)^{25}Mg reaction and ^{13}C pocket has been introduced. However, for the lowest mass stars we introduce some partial mixing of protons at the deepest extent of each third dredge-up episode in order to form a ^{13}C pocket (see detailed discussion in Lugaro et al. 2012). For most models the mass-loss rate used on the AGB is the semi-empirically derived Vassiliadis & Wood (1993) mass loss formulae. One of the major uncertainties in AGB modelling is the mass-loss rate, especially at the lowest metallicities, and for this reason we experiment with variations to the mass loss in the intermediate-mass AGB models. We refer to the discussions in Karakas (2010) and Karakas et al. (2012) for more details.

The s-process yields of massive rapid rotating stars are from Frischknecht et al. (2012); these results are more recent than Pignatari et al. (2008), and Frischknecht et al. (2012) based their yield predictions on a stellar evolution code. The code used is the Geneva stellar evolution code (GENEC), with reaction libraries from REACLIB, and neutron-captures from KADoNiS. Moreover, the results by Frischknecht et al. (2012) are based on the still favoured reaction rate for $^{17}O(\alpha,\gamma)$ by Caughlan & Fowler (1988). We explore the uncertainty linked to this reaction rate decreasing it by a factor of 10. In this way we can generate upper and lower limits for what we might expect as Sr yields from these massive rotating stars. In general the above mentioned s-process yields are of the order of $10^{-6} - 10^{-9} M_{\odot}$. (For comparison the non-rotating stars barely produce any Sr.)

5.2. The impact of different stellar yields on Galactic Chemical Evolution (GCE) models

We now show a chemical evolution model computed with the different assumptions for stellar yields discussed above. Because the goal of this section is to check for the broad impact of the different stellar yields on the chemical enrichment, we adopt a homogeneous chemical evolution model as guidance to our discussion. For that we use the halo chemical evolution model of Chiappini et al. (2008), which we briefly summarise here:
1) the infall law of the primordial gas follows a Gaussian function
2) the occurring outflow from the system is proportional to the star formation rate (SFR).

The timescale for the formation of the halo is fast (less than 0.5 Gyr). The other crucial element for our study is iron, for which we adopt the predictions from Woosley & Weaver 1995, (WW95). As shown in Cescutti & Chiappini (2010), this combination of parameters is able to produce a synthetic metallicity distribution function, which is in good agreement with the one observed in the Galactic halo (Lai et al. 2008; Schörck et al. 2009). Hence, we assume that this model follows the correct timescale for the chemical enrichment.

We have not run individual models for each set of AGB nucleosynthesis prediction. The reason is that even though our chemical evolution model calculates the enrichment from low-mass AGB stars and SNe Ia, only the more massive stars (SN II) can be considered drivers of the early chemical enrichment in the halo. This is due to the considerable longer timescales needed to evolve AGBs and SNe Ia. We have only tested the metal-poor yields for Sr (i.e. from the metal-poor extension to the yields from Lugaro et al. 2012); for which we have predictions up to $6M_{\odot}$ stars (compared to the $2 - 3M_{\odot}$ from Bisterzo et al. 2010; Cristallo et al. 2011). The massive AGB stars are more likely to contribute to the chemical enrichment during the formation of the halo, i.e. at lower metallicities. Nevertheless, the enrichment produced by the $6M_{\odot}$ AGB stars do not influence the overall results. Only when extremely low yields from even more massive stars (SN II) are adopted (see *Wlow*), it is possible to see the influence of the heavy AGB yields as a weak bump in the lower limit line around [Fe/H] $\sim$ -2 (see Fig. 11a) – top panel).

We have computed different chemical evolution models with different nucleosynthesis assumptions, namely:

- Case 1) Wanajo low yields (*Wlow*): $1.62{\cdot}10^{-9} M_{\odot}$ in the range 8-10$M_{\odot}$
- Case 2) Wanajo high (*Whigh*): $1.91{\cdot}10^{-3} M_{\odot}$ in the range 8-10$M_{\odot}$[3]
- Case 3) Arcones & Montes low (*AMlow*): $10^{-7} M_{\odot}$ mass range 8-25$M_{\odot}$
- Case 4) Arcones & Montes high (*AMhigh*): $10^{-4} M_{\odot}$ in mass range 8-25$M_{\odot}$[4]
- Case 5) Frischknecht low (*Flow*) with rotation and their 'standard' value for the reaction rate, generalising the production of the $25M_{\odot}$ in their paper to a range of 15-40$M_{\odot}$
- Case 6) Frischknecht high (*Fhigh*) calculated as Flow but with a decreased value for the reaction ^{17}O rate (producing higher Sr yields)

In Fig. 11a) (top) we show the models *Wlow* and *Whigh*, which differ in the level of Sr enrichment by the ECSN. The high level of Sr production in a small range of masses produces in the case of Whigh an important bump in the [Sr/Fe] predictions. This roughly appears as a knee in the [Sr/Fe] trend at [Fe/H]~ -3. However, the *Whigh* model produces too much Sr compared to the observed values. Including CEMP-s stars, we would have

[3] Wanajo standard (*Wstand*): $1.78{\cdot}10^{-4} M_{\odot}$ for the same range of masses

[4] Arcones & Montes standard (*Astand*): $10^{-4} M_{\odot}$ in mass range 12-25$M_{\odot}$ and $10^{-7} M_{\odot}$ in mass range 8-12$M_{\odot}$ and M$> 25M_{\odot}$.

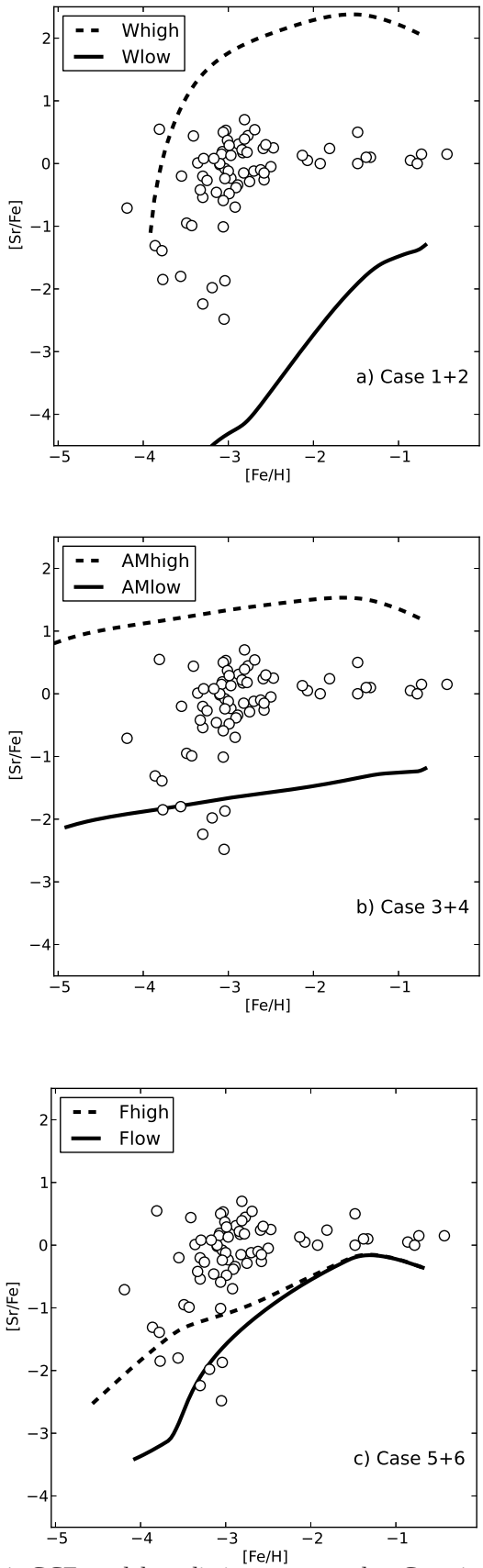

Fig. 11: GCE model predictions compared to Case 1+2) which is based on ECSN yields from S. Wanajo in the top panel a). The predictions are in the middle panel b) compared to Case 3+4) which is neutrino-driven winds from Arcones & Montes, and in the bottom panel c) the comparison is made to Case 5+6) namely fast rotating stars from U. Frischknecht. The dashed/solid lines represent the upper/lower limits to the Sr yields, respectively.

found some stars closer to the *Whigh* model at the lowest metallicity only. The *Wlow* model predicts too low [Sr/Fe] ratios at all [Fe/H] values compared to the observations. However, the AGB enrichment can be seen at $-2.3 <$ [Fe/H] < -1.5.

Model *AMlow* and *AMhigh* are presented in Fig. 11b) (middle). In these models the Sr is produced in a wide range of massive stars, which leads to a rather flat [Sr/Fe] trend. The nearly 3 dex difference between the upper and lower curves (*AMlow* and *AMhigh*) reflects the variations and uncertainties in the Sr yields.

From the results obtained from the two pairs of models we cannot draw strong conclusions as to the nucleosynthetic origin of Sr in our metal-poor star sample; the only message we can read from them is that some combination of two r-process sites, can roughly explain the observationally derived abundances. At this level, the observations/data can still be used to constrain the theoretical yields, rather than the other way around.

Finally, from the two models generated using the Frischknecht et al. (2012) yields (Fig. 11c) bottom panel), we can conclude that the s-process from fast rotating massive stars may be an important source of Sr during the Galactic halo formation (see Cescutti et al. 2013). The early s-process taking place in metal-poor, fast rotating, massive stars should be coupled/added to at least one r-process.

Since the difference between the LTE and NLTE Sr abundances is small, despite the slight horizontal shift caused by the positive NLTE effect on metallicity, the methodology does not impact on the interpretations in a GCE context (see Fig. 12). Therefore only the same GCE conclusions can be drawn under LTE and NLTE. We stress that this is only true for an element like Sr. Owing to the combined NLTE effects in Sr and Fe, there are no stars below [Fe/H] $=-3.5$ with high strontium abundances ([Sr/Fe]> 0). Our NLTE corrected abundances still show a large star-to-star scatter as is also found in Andrievsky et al. (2011).

Without precise theoretical yields it is impossible to draw firm conclusions based on the abundance measurements. On the other hand the presence of the spread can be explained in a stochastic chemical evolution scenario.

Many advances have been made in modelling AGB stars, SN, and the r-process as well as significant improvements in the determination of atomic data for heavy elements. These have in turn improved the GCE models. However, the r-process yields still need to be better constrained not to span 3-6 dex. Until these improvements are made, yield predictions should only be used as guiding upper and lower limits. The yields from the fast rotating stars and the AGB stars also face challenges when trying to constrict the ^{13}C pockets, pulse duration, mass loss, and poisons in order to improve the networks and in turn yields. Only within the last decade have SN models managed to explode, and the treatment of ^{13}C pockets and mass loss from AGB stars are improving (e.g. Matsuura et al. 2007; Mattsson et al. 2008; Sloan et al. 2012). For example, by using AGB stars in star clusters it is possible to constrain uncertain parameters related to convection and mass loss (e.g. Lebzelter et al. 2008; Kamath et al. 2012), while ^{13}C pocket sizes can be constrained using data from a variety of observational data (e.g., Lugaro et al. 2003; Bonačić Marinović et al. 2007; Bisterzo et al. 2012).

There are still many challenges including a detailed understanding of the formation mechanism of ^{13}C pockets, which is currently unknown and a significant uncertainty in s-process models of AGB stars (e.g., see discussion in Herwig 2005). The yields from fast rotating massive stars also face some of the same challenges including an accurate description of mass loss and convection in stellar models (e.g., see review by Langer 2012).

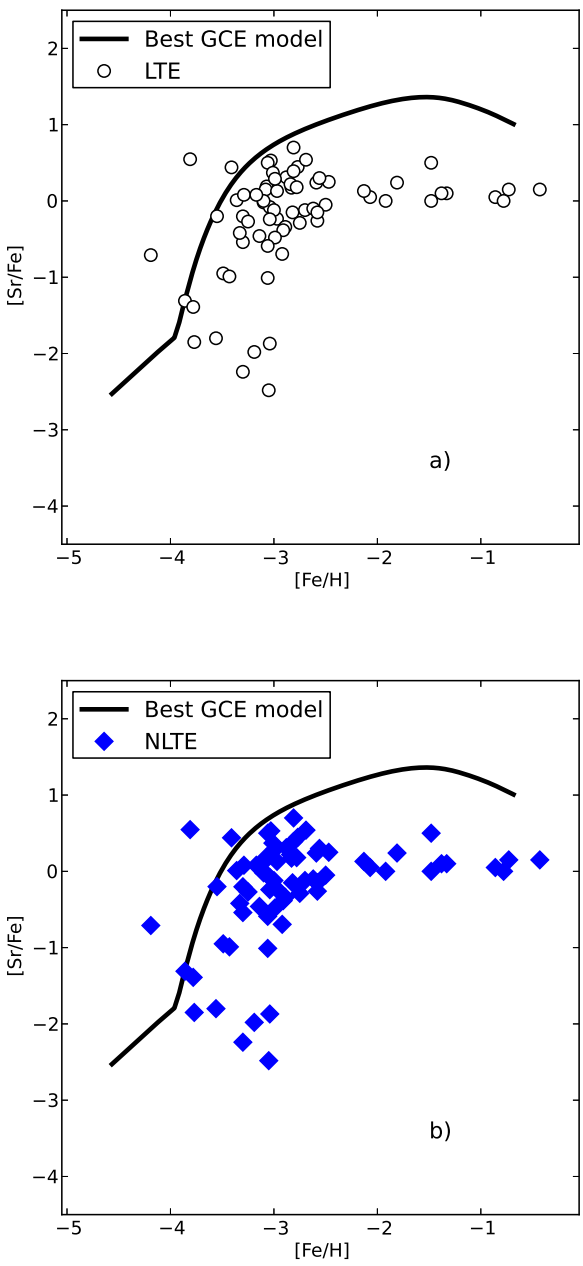

Fig. 12: Comparison of the best homogeneous GCE model (solid line) to Sr LTE abundances (open circles) in the upper panel a), and to NLTE Sr abundances (filled blue diamonds) in the lower panel b).

However, on the basis of Fig. 11 and 12 we believe that at least two different sources (e.g. neutrino-driven winds from massive stars or low mass ECSN) are needed to explain the [Sr/Fe] abundances we derived under both LTE and NLTE. An early s-process could take place in fast rotating stars and provide a possible explanation for the low [Sr/Fe] we obtain at very low metallicity.

6. Conclusions

Cross-disciplinary work is crucial to be able to compute better yields, and in turn better chemical evolution models. Only then will such calculations allow us to accurately predict the behaviour and evolution of the heavy elements such as Sr. This information is much needed in the era of high-resolution surveys, where we have a large flow of data coming. We are now capable of analysing the stars and extracting very accurate abundances with uncertainties < 0.25 dex, compared to what can be obtained from nucleosynthetic yields and evolved stellar models. This indicates that observationally derived abundances are more likely to constrain the parameter space of the yield predictions and the GCE models than vice versa.

On the basis of this study we can conclude the following about Sr in metal-poor stars.

- When deriving Sr I abundances, NLTE corrections should always be applied in order to obtain ionisation equilibrium.
- In the interval $-3.0 < [Fe/H] <\sim -1.0$ the chemical evolution of Sr, as derived from the Sr II resonance lines, is similar under LTE and NLTE. However, below [Fe/H] = −3.0 the NLTE corrections to Sr II lines are important to obtain the correct Sr abundances.
- The abundances obtained from the Sr II lines are sensitive to surface gravity. If the latter parameter is obtained from the ionisation equilibrium of Fe, LTE approximation should not be used, because it leads to large systematic errors in $\log g$ of up to +0.8 dex.
- In their current state the Sr yields are too uncertain to clearly disentangle contributions from different processes or sites. We may instead use the observationally derived abundances to constrain the parameter space of the model predictions.

In summary, it is not sufficient to account for NLTE effects in the line formation of the Sr lines. NLTE effects must be taken into account in the determination of stellar parameters, i.e., surface gravities and metallicities. Alternatively, abundances determined from the lines of the majority species, Sr II and Fe II, can be used. The LTE assumption is a trustworthy chemical evolution tracer, in the interval $-3 < [Fe/H] < 0$, for the Sr II abundances from dwarfs calculated with gravities stemming from parallaxes and temperatures based on accurate photometry. The metal-poor giants, which are the best targets at low metallicity, are biased by the LTE assumption. The parameters of the giants and their abundances must be computed under NLTE.

With the current uncertainties on the stellar yields, which span two to three orders of magnitude, we cannot draw strong conclusions on the chemical evolution of Sr in the early Galaxy. Neither can we precisely extract the various sites which contribute to the creation of the large star-to-star scatter, although at least two sites seem necessary. The yield predictions and the GCE model used in this work provide both upper and lower limits to the highly scattered stellar strontium abundances.

Acknowledgements. This work was supported by Sonderforschungsbereich SFB 881 "The Milky Way System" (subproject A5) of the German Research Foundation (DFG). Based on observations made with the European Southern Observatory telescopes (obtained from the ESO/ST-ECF Science Archive Facility) and the Calar Alto Observatory telescopes. We are grateful to R. Schönrich for useful discussions, to S. Bisterzo for yields, and to L. Sbordone for comments. We thank T. Gehren for providing spectra, and S. Wanajo for ECSN yields. A.A. is supported by the Helmholtz-University Young Investigator grant No. VH-NG-825. Finally, we thank the referee for the detailed comments.

References

Alonso, A., Arribas, S., & Martinez-Roger, C. 1996, A&A, 313, 873

Alonso, A., Arribas, S., & Martínez-Roger, C. 1999, A&AS, 140, 261
Anders, E. & Grevesse, N. 1989, Geochim. Cosmochim. Acta, 53, 197
Andrievsky, S. M., Spite, F., Korotin, S. A., et al. 2011, A&A, 530, A105
Andrievsky, S. M., Spite, M., Korotin, S. A., et al. 2009, A&A, 494, 1083
Arcones, A., Janka, H.-T., & Scheck, L. 2007, aap, 467, 1227
Arcones, A. & Montes, F. 2011, ApJ, 731, 5
Beers, T. C. & Christlieb, N. 2005, ARA&A, 43, 531
Belyakova, E. V. & Mashonkina, L. I. 1997, Astronomy Reports, 41, 530
Bergemann, M. & Gehren, T. 2008, A&A, 492, 823
Bergemann, M., Hansen, C. J., Bautista, M., & Ruchti, G. 2012a, A&A, 546, A90
Bergemann, M., Lind, K., Collet, R., Magic, Z., & Asplund, M. 2012b, MNRAS, 427, 27
Bisterzo, S., Gallino, R., Straniero, O., Cristallo, S., & Käppeler, F. 2010, MNRAS, 404, 1529
Bisterzo, S., Gallino, R., Straniero, O., Cristallo, S., & Käppeler, F. 2012, MNRAS, 422, 849
Bonačić Marinović, A., Lugaro, M., Reyniers, M., & van Winckel, H. 2007, A&A, 472, L1
Bonifacio, P., Monai, S., & Beers, T. C. 2000, AJ, 120, 2065
Bonifacio, P., Spite, M., Cayrel, R., et al. 2009, A&A, 501, 519
Busso, M., Gallino, R., & Wasserburg, G. J. 1999, ARA&A, 37, 239
Butler, K. & Giddings, J. 1985, Newsletter on Analysis of Astronomical Spectra No. 9 (University College London)
Casagrande, L., Ramírez, I., Meléndez, J., Bessell, M., & Asplund, M. 2010, A&A, 512, A54
Caughlan, G. R. & Fowler, W. A. 1988, Atomic Data and Nuclear Data Tables, 40, 283
Cescutti, G. 2008, A&A, 481, 691
Cescutti, G. & Chiappini, C. 2010, A&A, 515, A102
Cescutti, G., Chiappini, C., Hirschi, R., Meynet, G., & Frischknecht, U. 2013, A&A, Submitted,
Chiappini, C., Ekström, S., Meynet, G., et al. 2008, A&A, 479, L9
Chiappini, C., Frischknecht, U., Meynet, G., et al. 2011, Nature, 472, 454
Collet, R., Asplund, M., & Trampedach, R. 2007, A&A, 469, 687
Cristallo, S., Piersanti, L., Straniero, O., et al. 2011, ApJS, 197, 17
Dekker, H., D'Odorico, S., Kaufer, A., Delabre, B., & Kotzlowski, H. 2000, in Proc. SPIE, Vol. 4008, 534
Dobrovolskas, V., Kucinskas, A., Andrievsky, S. M., et al. 2012, A&A, 540,
Fischer, T., Whitehouse, S. C., Mezzacappa, A., Thielemann, F., & Liebendörfer, M. 2010, aap, 517, A80+
François, P., Depagne, E., Hill, V., et al. 2007, A&A, 476, 935
Frischknecht, U., Hirschi, R., & Thielemann, F.-K. 2012, A&A, 538, L2
Gehren, T., Liang, Y. C., Shi, J. R., Zhang, H. W., & Zhao, G. 2004, A&A, 413, 1045
Gehren, T., Shi, J. R., Zhang, H. W., Zhao, G., & Korn, A. J. 2006, A&A, 451, 1065
González Hernández, J. I., Bonifacio, P., Ludwig, H.-G., et al. 2010, A&A, 519, A46
Grupp, F. 2004a, A&A, 420, 289
Grupp, F. 2004b, A&A, 426, 309
Gustafsson, B., Edvardsson, B., Eriksson, K., et al. 2008, A&A, 486, 951
Hansen, C. J., Primas, F., Hartman, H., et al. 2012, A&A, 545, A31
Heil, M., Juseviciute, A., Käppeler, F., et al. 2009, PASA, 26, 243
Herwig, F. 2005, ARA&A, 43, 435
Hoffman, R. D., Woosley, S. E., & Qian, Y.-Z. 1997, ApJ, 482, 951
Kamath, D., Karakas, A. I., & Wood, P. R. 2012, ApJ, 746, 20
Käppeler, F., Beer, H., & Wisshak, K. 1989, RPPh, 52, 945
Karakas, A. I. 2010, MNRAS, 403, 1413
Karakas, A. I., García-Hernández, D. A., & Lugaro, M. 2012, ApJ, 751, 8
Lai, D. K., Bolte, M., Johnson, J. A., et al. 2008, ApJ, 681, 1524
Langer, N. 2012, ARA&A, 50, 107
Lebzelter, T., Lederer, M. T., Cristallo, S., et al. 2008, A&A, 486, 511
Lind, K., Bergemann, M., & Asplund, M. 2012, ArXiv e-prints
Lugaro, M., Davis, A. M., Gallino, R., et al. 2003, ApJ, 593, 486
Lugaro, M., Karakas, A. I., Stancliffe, R. J., & Rijs, C. 2012, ApJ, 747, 2
Martínez-Pinedo, G., Fischer, T., Lohs, A., & Huther, L. 2012, ArXiv e-prints
Masana, E., Jordi, C., & Ribas, I. 2006, A&A, 450, 735
Mashonkina, L., Gehren, T., & Bikmaev, I. 1999, A&A, 343, 519
Matsuura, M., Zijlstra, A. A., Bernard-Salas, J., et al. 2007, MNRAS, 382, 1889
Mattsson, L., Wahlin, R., Höfner, S., & Eriksson, K. 2008, A&A, 484, L5
Nissen, P. E., Akerman, C., Asplund, M., et al. 2007, A&A, 469, 319
Nissen, P. E., Hoeg, E., & Schuster, W. J. 1997, in Hipparcos - Venice '97, Vol. 402 (ESA Special Publication), 225
Nissen, P. E., Primas, F., Asplund, M., & Lambert, D. L. 2002, A&A, 390, 235
Önehag, A., Gustafsson, B., Eriksson, K., & Edvardsson, B. 2009, A&A, 498, 527
Pignatari, M., Gallino, R., Heil, M., et al. 2010, ApJ, 710, 1557
Pignatari, M., Gallino, R., Meynet, G., et al. 2008, ApJ, 687, L95
Ramírez, I. & Meléndez, J. 2005, ApJ, 626, 465
Reetz, J. 1999, PhD thesis, LMU Münich
Roberts, L. F. 2012, ApJ, 755, 126
Roberts, L. F. & Reddy, S. 2012, ArXiv e-prints
Sbordone, L., Bonifacio, P., Caffau, E., et al. 2010, A&A, 522, A26
Schlegel, D. J., Finkbeiner, D. P., & Davis, M. 1998, ApJ, 500, 525
Schörck, T., Christlieb, N., Cohen, J. G., et al. 2009, A&A, 507, 817
Sloan, G. C., Matsuura, M., Lagadec, E., et al. 2012, ApJ, 752, 140
Sneden, C., Cowan, J. J., & Gallino, R. 2008, ARA&A, 46, 241
Spite, M., Andrievsky, S. M., Spite, F., et al. 2012, A&A, 541, A143
Taylor, J. 1997, An Introduction to Error Analysis (University Science Books)
Travaglio, C., Gallino, R., Arnone, E., et al. 2004, ApJ, 601, 864
Vassiliadis, E. & Wood, P. R. 1993, ApJ, 413, 641
Vogt, S. S., Allen, S. L., Bigelow, B. C., et al. 1994, in Proc. SPIE, Vol. 2198, 362
Wanajo, S., Janka, H., & Mueller, B. 2010, ArXiv e-prints
Woosley, S. E. & Weaver, T. A. 1995, ApJS, 101, 181

Appendix A: Abundance Details

Here we show the LTE and the NLTE abundances as well as parameters. The abundance is given for 4077Å and 4607Å individually.

Table A.1: Sr abundances for the sample of stars.

LTE	LTE parameters			EW	Syn		NLTE parameters		NLTE EW	Syn	Corr.	Full NLTE	Syn	Corr.	Full NLTE
Star	T	logg	[Fe/H]	4077	4077	4607	logg	[Fe/H]	4077	4077	ΔNLTE	4077	4607	ΔNLTE	4607
HD134169	5930.	3.98	–	–	0.05	−0.15	3.98	−0.86	–	0.05	−0.01	0.040	–	–	0.09
HD148816	5880.	4.07	–	–	0.00	−0.25	4.07	−0.78	–	0.00	−0.01	−0.01	–	–	0.01
HD184448	5765	4.16	–	–	0.15	−0.15	4.16	−0.43	–	0.15	−0.01	0.14	–	–	0.05
HD3567	6035.	4.08	−1.33	−0.04	0.1	< −0.3	4.08	−1.29	−0.1	0.14	−0.02	0.12	< −0.35	0.28	< −0.07
HD19445	5982.	4.38	−2.13	−0.05	0.13	< 0.14	4.38	−2.10	−0.12	0.11	−0.05	0.06	< 0.05*	0.34	< 0.39*
HD106038	5950.	4.33	−1.48	0.65	0.5	0.33	4.33	−1.45	0.6	0.5	−0.02	0.48	0.3	0.3	0.6
HD121004	5711.	4.46	−0.73	0.21	0.15	0.2	4.46	−0.71	0.2	0.15	−0.01	0.14	0.14	0.24	0.38
HD122196	6048.	3.89	−1.81	0.05	0.24	–	3.89	−1.75	−0.01	0.22	−0.03	0.19	–	–	
HD122563	4665	1.65	−2.60	−0.09	−0.05	< −0.6	1.65	−2.50	−0.09	−0.05	0.0	−0.05	< −0.7	0.45	< −0.25
HD140283	5777	3.70	−2.58	−0.33	−0.15	–	3.70	−2.38	−0.54	−0.36	−0.01	−0.37	–	–	–
HD175305	5100.	2.70	−1.38	−0.02	0.1	−0.35	2.70	−1.34	−0.06	0.11	0.0	0.11	−0.4	0.37	−0.03
G6412	6464	4.30	−3.24	−0.05	0.0	–	4.30	−3.12	0.04	0.05	0.12	0.17	–	–	–
G6437	6494.	3.82	−3.17	−0.09	0.08	–	4.23	−3.00	−0.05	0.08	0.09	0.17	–	–	–
BD133442	6450.	4.20	−2.56	0.26	0.3	–	4.42	−2.47	0.14	0.27	−0.06	0.21	–	–	–
CS30312-059	5021.	1.90	−3.06	0.46	0.5	–	2.41	−2.89	0.28	0.35	−0.04	0.31	–	–	–
CS31082-001	4925.	1.51	−2.81	0.59	0.7	–	2.05	−2.63	0.65	0.62	−0.02	0.6	–	–	–
HD74462	4590.	1.84	−1.48	0.1	0.0	−0.5	1.98	−1.43	0.04	−0.12	0.0	−0.12	−0.5	0.34	−0.16
HD126238	4900	1.80	−1.92	0.02	0.0	−0.34	2.02	−1.85	0.03	0.05	0.0	0.05	−0.46	0.43	−0.03
HD126587	4950.	1.90	−3.01	0.39	0.37	< −0.05	2.36	−2.86	0.34	0.25	−0.04	0.21	< −0.15	0.4	< 0.25
HE0315+0000	5050.	2.05	−2.81	0.17	0.39	–	2.47	−2.67	0.03	0.26	−0.03	0.23	–	–	–
HE1219-0312	5100.	2.05	−2.99	0.22	0.29	–	2.58	−2.81	0.08	0.17	−0.05	0.12	–	–	–

Notes. (*) Larger uncertainty ±0.1 dex in measurement
(<) upper limit on the abundance